Transient layers in the topside ionosphere of Mars

A. J. Kopf,[1] D. A. Gurnett,[1] D. D. Morgan,[1] and D. L. Kirchner[1]

Received 6 June 2008; revised 23 July 2008; accepted 25 July 2008; published 13 September 2008.

[1] Radar soundings from the MARSIS instrument on board the Mars Express spacecraft have shown that distinct layers can occur in the topside ionosphere of Mars, well above the main photo-ionization layer. These layers appear as cusps, or sometimes steps, in plots of the time delay as a function of frequency. Usually only one topside layer is observed, typically at altitudes from 180 to 240 km. However, occasionally an additional layer occurs at even higher altitudes. The layers are transient features and are present about 60% of the time near the subsolar point, decreasing with increasing solar zenith angle to less than 5% at the terminator and the nightside. The transient nature of the layers suggests that they are produced by a dynamical process, most likely involving an interaction with the solar wind in the upper levels of the ionosphere. **Citation:** Kopf, A. J., D. A. Gurnett, D. D. Morgan, and D. L. Kirchner (2008), Transient layers in the topside ionosphere of Mars, *Geophys. Res. Lett.*, *35*, L17102, doi:10.1029/2008GL034948.

1. Introduction

[2] The Mars Express spacecraft [*Chicarro et al.*, 2004] carries a low-frequency radar called the Mars Advanced Radar for Subsurface and Ionosphere Sounding (MARSIS) that is designed to sound the subsurface and ionosphere of Mars [*Picardi et al.*, 2004]. Spacecraft radar sounders, developed in the 1960s to study Earth's ionosphere [*Calvert*, 1966], have proven to be a powerful tool for studying planetary ionospheres. Before MARSIS, most knowledge of the Martian ionosphere came from radio occultation measurements [*Zhang et al.*, 1990; *Pätzold et al.*, 2005]. MARSIS data complement occultations by providing better spatial resolution and the ability to explore regions where occultations cannot be performed. In an overview of early MARSIS ionospheric results *Gurnett et al.* [2008] discussed the existence of a second layer in the ionosphere at an altitude near 200 km, well above the main photo-ionization layer, which occurs at 120 to 140 km [*Morgan et al.*, 2008]. In this paper we present a study of the second layer, and report the discovery of a third layer.

[3] Before discussing new results, it is useful to give a review of ionospheric sounding. A horizontally stratified ionosphere provides a nearly perfect reflecting surface for radar sounding. The radar pulse cannot propagate at frequencies below the plasma frequency,

$$f_p = 8980\sqrt{n_e}\text{Hz} \tag{1}$$

where n_e is the electron density in cm^{-3} [*Gurnett and Bhattacharjee*, 2005], and thus is reflected once it reaches the altitude where the wave frequency equals the plasma frequency. For frequencies above the maximum plasma frequency, the pulse passes through the ionosphere and is reflected by the surface of the planet as illustrated in the top plot of Figure 1.

[4] Ionospheric sounding data are usually displayed as an ionogram, which plots the reflected wave intensity as a function of transmitted frequency and time delay of the received echo. A sketch of the reflection trace from a typical ionogram is shown in the bottom plot of Figure 1. The scale on the left is time delay, Δt, plotted positive downward. The scale on the right, "apparent range," is the distance to the reflection point, $c\Delta t/2$, which assumes the pulse travels at the speed of light. The maximum plasma frequency in the ionosphere, $f_p(max)$, can be identified from the discontinuity in the echo trace labeled "cusp". The vertex of the cusp, which defines the boundary between the ionospheric and ground reflections, is caused by long time delays that occur as the wave propagates through the extended region where the wave frequency is close to the maximum plasma frequency. Cusps occur when the electron density has a local maximum, i.e., when $\partial n_e/\partial z = 0$, see *Budden* [1961]. If the surface reflection is too weak, then only the ionospheric half of the cusp is detected. This condition often occurs at solar zenith angles (SZA) less than about 60° and during solar energetic particle events [*Morgan et al.*, 2006].

[5] The apparent range gives a rough estimate of the distance to the reflection point, but accurate measurements require accounting for the deviation from the speed of light due to ionospheric plasma. Assuming vertical reflection from a horizontally stratified ionosphere, the time delay as a function of frequency is given by

$$\Delta t(f) = \frac{2}{c}\int_{z(f_p)}^{z_{sc}} \frac{dz}{\sqrt{1-\left(f_p(z)/f\right)^2}} \tag{2}$$

where z_{sc} is the altitude of the spacecraft and $z(f_p)$ is the altitude of the reflection point [*Gurnett et al.*, 2005]. If the electron density is assumed to be monotonic with altitude, then the measured time delay, $\Delta t(f)$, can be inverted to give the plasma frequency (or electron density) as a function of altitude, $f_p(z)$, see *Budden* [1961]. Because of the monotonic requirement, a unique inversion cannot be obtained if there are distinct layers separated by points where $\partial n_e/\partial z = 0$, though limits can be put on such inversions.

2. Topside Layers

[6] In addition to the cusp associated with the main ionospheric layer, many MARSIS ionograms have a second cusp at a substantially lower frequency, indicating the

[1]Department of Physics and Astronomy, University of Iowa, Iowa, USA.

0094-8276/08/2008GL034948$05.00

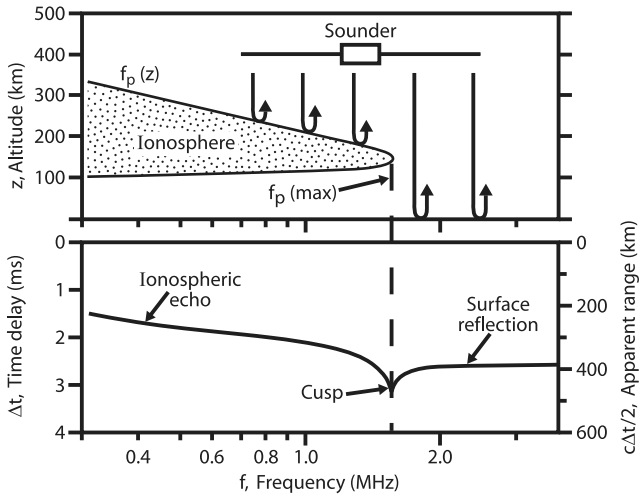

Figure 1. (top) Frequency dependent reflection of a radar signal from the topside of the Martian ionosphere and (bottom) the resulting time delay of the reflected signal as a function of frequency. The cusp in the trace at f_p(max) is caused by the very low group velocity and long path length near the peak in the density profile, where $\partial n_e/\partial z = 0$.

presence of a second layer well above the main layer. An example is shown in Figure 2a. The maximum plasma frequency of the second layer is the frequency at the vertex of the cusp, 1.65 MHz in this case, which using equation (1) yields a peak electron density of 3.37×10^4 cm^{-3} for the second layer. Sometimes the vertex is missing and the second layer can only be identified by a distinct downward step in the trace with increasing frequency, as in Figure 2b.

[7] Inspection of many examples reveals that the maximum electron density of the second layer is highly variable. To illustrate this, Figure 3 plots the apparent altitude of the ionospheric reflection as a function of electron density and time for a typical dayside pass. Here, apparent altitude is defined as the spacecraft altitude minus the apparent range, i.e., $z = z_{sc} - c\Delta t/2$, where z_{sc} is the spacecraft altitude. It should be noted that apparent altitude is not a "real" altitude scale, in the sense that it has not been corrected for plasma effects, so its literal results can often be non-physical. However, we have found it to be by far the best scale to use to display the presence of these features. The scale on the right is the frequency of the sounding pulse, and the scale on the left is the corresponding density. The peak density of the second layer, n_e(max, main layer), can be identified from the irregular boundary defined by isolated cusps (green) and downward steps (usually red to yellow) in the apparent altitude. Not only does the boundary fluctuate

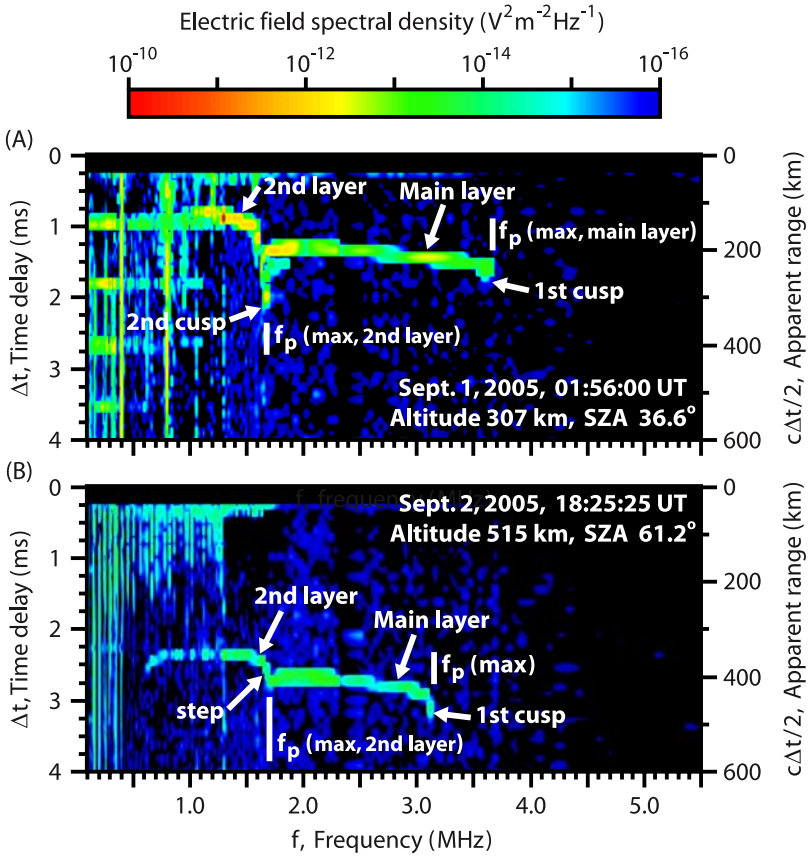

Figure 2. Two ionograms that show the presence of a second layer above the main ionospheric layer. (a) Ionogram showing a cusp with a vertex, indicating the presence of a peak in the density profile, hence a well-defined second layer, at an altitude well above the peak of the main layer. (b) Ionogram showing a step without a cusp-shaped vertex, which means that there is a region where $\partial n_e/\partial z$ is near zero, i.e., an inflection point rather than a clearly defined peak in the density profile.

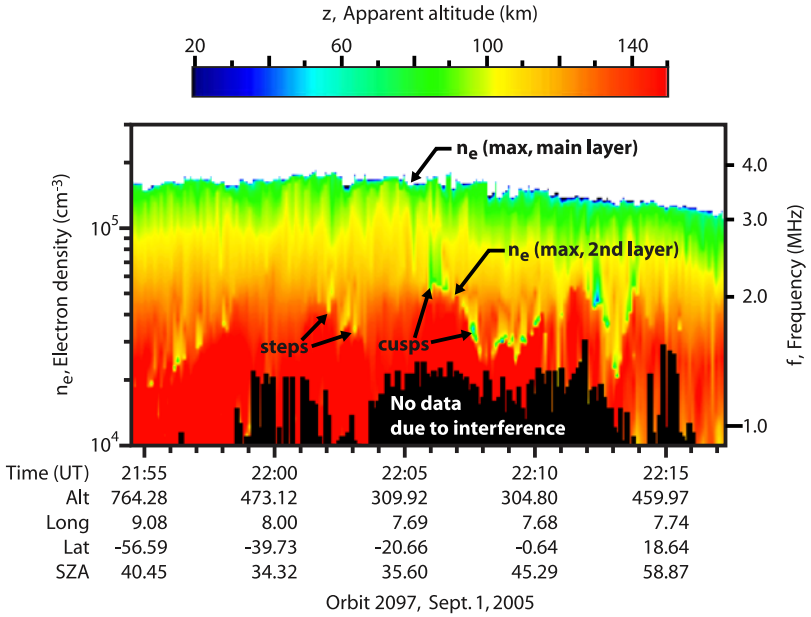

Figure 3. A spectrogram that shows the transient variations in the electron density of the second layer during a low altitude pass over the ionosphere. The color coding gives the apparent altitude of the reflection, which is the spacecraft altitude minus the apparent range, $c\Delta t/2$. The irregular boundary defined by the cusps and steps gives the maximum electron density of the second layer, n_e (max, 2nd layer).

considerably, from about (2 to 5) $\times$ 10^4 cm^{-3}, but it also disappears completely at times, indicating the second layer is a transient phenomenon. The fluctuation time scale varies considerably, from tens of seconds to several minutes, equal to spatial scales from a few tens to several hundred km. These fluctuations are in sharp contrast to the maximum electron density of the main layer, n_e(max, main layer), which is quite smooth and continuous over the entire pass. The transient layers are observed on nearly every dayside pass.

[8] To study the statistical properties of the second layer, roughly 4000 ionograms have been analyzed for the orbits during the period from August 5, 2005, to September 5, 2005, including approximately 1500 ionograms which show the second layer. These orbits cover a wide range of latitudes and longitudes, and solar zenith angles from near the subsolar point (SZA = 0°) to the terminator (SZA = 90°). Figure 4 shows the probability of occurrence, the maximum electron density, and the altitude of the second layer, all as a function of SZA. The probability of occurrence has a broad maximum of about 60% near the subsolar point and decreases with increasing SZA to less than 5% at the terminator. The maximum electron density of the layer ranges from about (2 to 7) $\times$ 10^4 cm^{-3} and the altitude of the maximum density varies from about 180 to 220 km, with an average of about 200 km. There appears to be a slight tendency for the maximum electron density to decrease, and the altitude of the maximum to increase, with increasing SZA. The occurrence probability shows no relationship to surface features, or to the crustal magnetic fields discovered by *Acuña et al.* [1999]. Also, there is no clear relationship to variations in the solar EUV radiation as monitored via the F10.7 solar radio flux, or to solar energetic particle events.

[9] Figure 5a shows an ionogram with a third cusp (or step) indicating the presence of a third layer above a well defined second layer. The electron density profile, Figure 5b, has been computed by inverting equation (2). Since the

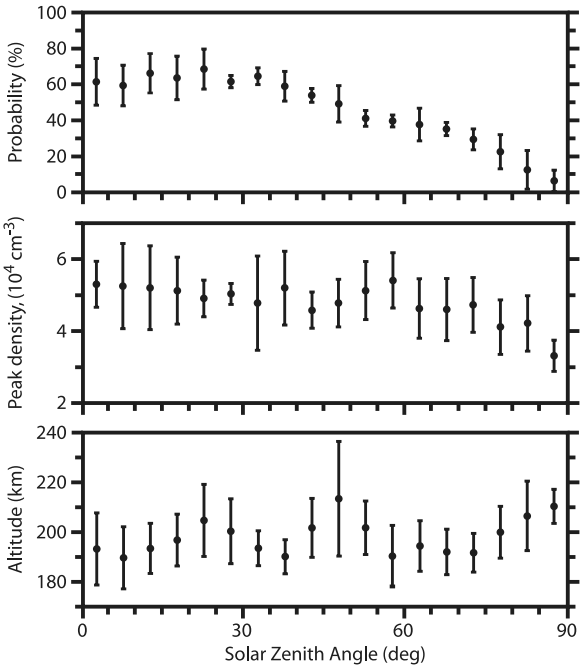

Figure 4. A statistical summary of the properties of the second layer: (top) occurrence probability, (middle) maximum electron density, and (bottom) altitude of the maximum computed by inverting equation (2), all as a function of solar zenith angle.

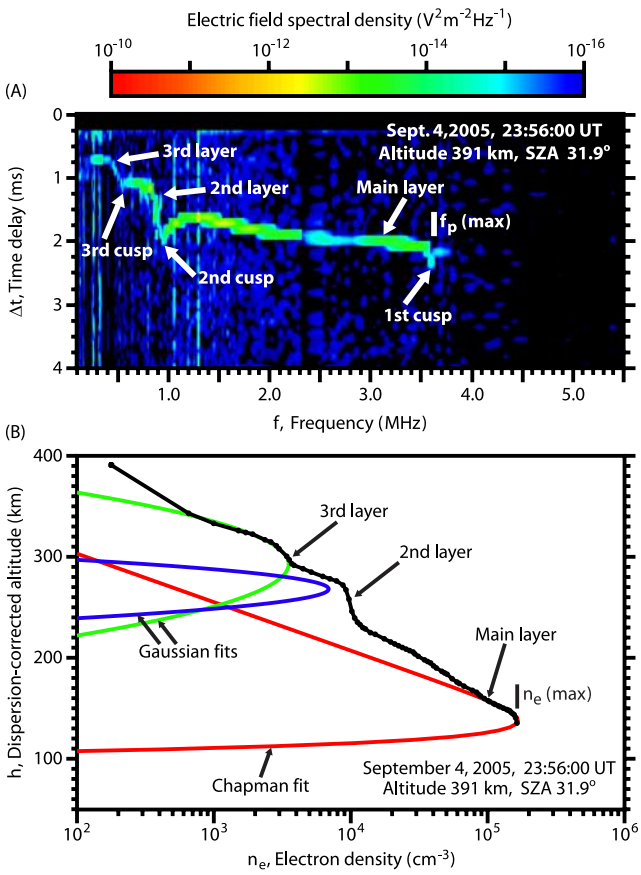

Figure 5. (a) Ionogram with the characteristic signature of a third topside layer. (b) Corresponding electron density profile computed by inverting equation (2). The computation was performed assuming a monotonic density profile.

presence of topside layers leads to indeterminacy in the inversion process, we have arbitrarily assumed the density profile to be a continuous monotonic function across the interfaces between layers. This assumption gives an upper altitude limit to the true profile. The resulting inversion places the peak of the main layer at 138 km with a maximum density of 1.66×10^5 cm^{-3}. These parameters are close to the nominal values given by *Morgan et al.* [2008] for the main layer at this SZA (31.9°). This good agreement with previous results gives us confidence that the computed profile is close to the true profile. The red line shows a fit to the Chapman photo-equilibrium equation [*Chapman*, 1931] for the main layer, and the blue and green lines show Gaussian fits to the electron density profile for the second and third layers. The vertical total electron content (TEC) for the main, second, and third layers are 7.17×10^{11}, 1.72×10^{10}, and 2.34×10^{10} cm^{-2}, respectively. These TEC values show that the total number of electrons in the topside layers is quite small, ~6%, compared to the main layer. Third layers are rare, detected only about 1% of the time, and as with the second layer are highly transient.

3. Interpretation

[10] When the second layer was first discovered, we thought it could be related to the O^+ layer discovered by Viking [*Hanson et al.*, 1977] at an altitude near 225 km. However, the vertical thickness of this O^+ layer, about 100 km, seems too large to account for the discrete topside layers detected by MARSIS, which have thicknesses of only a few tens of km (see Figure 5). Also, since O^+ production is an equilibrium process, this could not account for the transient behavior of the topside layers. Instead, this transience is indicative of a dynamical process in the upper ionosphere of Mars. Recently, local electron density measurements reported by *Duru et al.* [2008] from electron plasma oscillations excited by MARSIS have shown that at altitudes above 275 km the electron density is highly variable, with fluctuations often exceeding 25% in the range from 300 to 350 km, and even larger at higher altitudes. The transient topside layers detected by MARSIS soundings are most likely a manifestation of these fluctuations.

[11] Several possibilities exist for exciting such fluctuations. *Wang and Nielsen* [2002] have suggested that fluctuations in solar wind ram pressure could excite large amplitude magnetohydrodynamic waves in the upper ionosphere, especially near the subsolar point where solar wind pressure variations are largest. Such waves have been observed in radio occultation data [*Wang and Nielsen*, 2003] at altitudes from about 145 to 200 km. Since nonlinearities often cause large amplitude waves to curl over and break, it is possible that such structures could appear as distinct layers to a radar sounder. The dayside source of these waves would be consistent with the observed SZA dependence of the transient topside layers, which occur most frequently near the subsolar point. Still, it is not clear that solar wind pressure fluctuations occur with sufficient amplitude and over the broad range of time scales needed to explain the near continuous presence of the transient topside layers.

[12] Because of the velocity shear between the solar wind and the ionosphere of an unmagnetized planet, various researchers have suggested that large amplitude waves could be generated in the upper ionosphere via the Kelvin-Helmholtz instability [see, e.g., *Terada et al.*, 2002]. *Penz et al.* [2004] have argued that large amplitude waves generated by this instability could play an important role in the loss of ions from the upper ionosphere of Mars. Since Kelvin-Helmholtz waves evolve into nonlinear structures with a curl-over and form detached plasma clouds, such structures could appear as distinct layers to a radar sounder. However, this mechanism is expected to be most unstable near the terminator, where the velocity shear is large, and may be stable near the subsolar point where the velocity shear is small. This trend is in disagreement with the SZA dependence in Figure 4, since the nature of the instability would suggest it would be more likely to appear toward the terminator rather than the subsolar point. However, further study is needed to see if this disagreement is sufficiently serious to rule out the Kelvin-Helmholtz mechanism.

[13] In addition to nonlinear wave mechanisms there are other solar wind related processes that could affect the density in the upper ionosphere. For example, magnetic reconnection near the nose of the induced magnetosphere could lead to enhanced transport of plasma out of the ionosphere [*Eastwood et al.*, 2008]. Also, it has been shown that the $\mathbf{v} \times \mathbf{B}$ electric field due to the bulk motion of the solar wind can cause plasma loss by accelerating ions out of

the ionosphere [*Modolo et al.*, 2005]. Clearly, further study is needed to determine which, if any, of the above processes are involved in the formation of topside layers.

[14] **Acknowledgments.** This research was supported by NASA through contract 1224107 with the Jet Propulsion Laboratory.

References

Acuña, M. H., et al. (1999), Global distribution of crustal magnetization discovered by the Mars Global Surveyor MAG/ER experiment, *Science*, *284*, 790–793.

Budden, K. G. (1961), *Radio Waves in the Ionosphere*, pp. 160–162, Cambridge Univ. Press, Cambridge, U. K.

Calvert, W. (1966), Ionospheric topside soundings, *Science*, *154*, 228–234.

Chapman, S. (1931), The absorption and dissociative or ionizing effect of monochromatic radiation in an atmosphere on a rotating Earth part II. Grazing incidence, *Proc. Phys. Soc.*, *43*, 483–501, doi:10.1088/0959-5309/43/5/302.

Chicarro, A., P. Martin, and R. Traunter (2004), The Mars Express mission: An overview, in *Mars Express: The Scientific Payload*, edited by A. Wilson, *Eur. Space Agency Spec. Publ.*, *SP-1240*, 3–16.

Duru, F., D. A. Gurnett, D. D. Morgan, R. Modolo, A. F. Nagy, and D. Najib (2008), Electron densities in the upper ionosphere of Mars from the excitation of electron plasma oscillations, *J. Geophys. Res.*, *113*, A07302, doi:10.1029/2008JA013073.

Eastwood, J. P., D. A. Brain, J. S. Halekas, J. F. Drake, T. D. Phan, M. Øieroset, D. L. Mitchell, R. P. Lin, and M. Acuña (2008), Evidence for collisionless magnetic reconnection at Mars, *Geophys. Res. Lett.*, *35*, L02106, doi:10.1029/2007GL032289.

Gurnett, D. A., and A. Bhattacharjee (2005), *Introduction to Plasma Physics*, Cambridge Univ. Press, Cambridge, U. K.

Gurnett, D. A., et al. (2005), Radar soundings of the ionosphere of Mars, *Science*, *310*, 1929–1933, doi:10.1126/science.1121868.

Gurnett, D. A., et al. (2008), An overview of radar soundings of the Martian ionosphere from the Mars Express spacecraft, *Adv. Space Res.*, *41*, 1335–1346, doi:10.1016/j.asr.2007.01.062.

Hanson, W. B., S. Sanatani, and D. R. Zuccaro (1977), The Martian ionosphere as observed by the Viking retarding potential analyzers, *J. Geophys. Res.*, *82*, 4351–4363.

Modolo, R., G. M. Chanteur, E. Dubinin, and A. P. Matthews (2005), Influence of the solar EUV flux on the Martian plasma environment, *Ann. Geophys.*, *23*, 433–444.

Morgan, D. D., D. A. Gurnett, D. L. Kirchner, R. L. Huff, D. A. Brain, W. V. Boynton, M. H. Acuña, J. J. Plaut, and G. Picardi (2006), Solar control of radar wave absorption by the Martian ionosphere, *Geophys. Res. Lett.*, *33*, L13202, doi:10.1029/2006GL026637.

Morgan, D. D., D. Gurnett, D. L. Kirchner, J. L. Fox, E. Nielsen, and J. J. Plaut (2008), Variation of the Martian ionospheric electron density from Mars Express radar soundings, *J. Geophys. Res.*, doi:10.1029/2008JA013313, in press.

Pätzold, M., S. Tellmann, B. Häusler, D. Hinson, R. Schaa, and G. L. Tyler (2005), A sporadic third layer in the ionosphere of Mars, *Science*, *310*, 837–839.

Penz, T., et al. (2004), Ion loss on Mars caused by the Kelvin-Helmholtz instability, *Planet. Space Sci.*, *52*, 1157–1167.

Picardi, G., et al. (2004), MARSIS: Mars advanced radar for subsurface and ionosphere sounding, in *Mars Express: The Scientific Payload*, edited by A. Wilson, Eur. Space Agency Spec. Publ., SP-1240, 51–70.

Terada, N., S. Machida, and H. Shinagawa (2002), Global hybrid simulation of the Kelvin-Helmholtz instability at the Venus ionopause, *J. Geophys. Res.*, *107*(A12), 1471, doi:10.1029/2001JA009224.

Wang, J.-S., and E. Nielsen (2002), Dispersion relation and numerical simulation of hydrodynamic waves in Mars' topside ionosphere, paper presented at 27th General Assembly, Eur. Geophys. Soc., Nice, France.

Wang, J.-S., and E. Nielsen (2003), Wavelike structures in the Martian topside ionosphere observed by Mars Global Surveyor, *J. Geophys. Res.*, *108*(E7), 5078, doi:10.1029/2003JE002078.

Zhang, M. G. H., J. G. Luhmann, and A. J. Kilore (1990), A post Pioneer Venus reassessment of the Martian dayside ionosphere as observed by radio occultation methods, *J. Geophys. Res.*, *95*, 14,829–14,839.

D. A. Gurnett, D. L. Kirchner, A. J. Kopf, and D. D. Morgan, Department of Physics and Astronomy, University of Iowa, Iowa City, IA 52242, USA. (andrew-kopf@uiowa.edu)